Suppression of Cavitation and Unstable Flow in Throttled Turbopumps

GEORGE S. WONG,* CHARLES A. MACGREGOR,† AND ROBERT K. HOSHIDE‡
North American Aviation, Inc., Canoga Park, Calif.

This paper describes a system in which high-energy fluid is tapped from the discharge of a turbopump and injected tangentially upstream of its inducer to improve flow distribution and suppress cavitation and instabilities that occur when the turbopump is throttled. In various tests of inducers in a water tunnel and of a complete experimental pump, the critical suction specific speed was increased by 20 to 50%. Here the critical S_s is defined as the value at which there is a 2% loss in pump head due to cavitation. The critical S_s is related to $(NPSH_{cr})^{-3/4}$ and, accordingly, the net positive suction head was reduced by 15 to 40% for a given throttled pump output. Unstable flow in the pump was reduced over the cavitating and noncavitating flow range. Typically, good results were obtained with approximately 10% bleed flow injected tangentially from a nozzle ring 1 diam upstream of the inducer and with injection angles relative to the wall of $\theta_j = 0°$ (tangential) and $\gamma_j = 45°$ to $60°$ (axial, downstream). The system, although tested only with water to date, shows promise for application to throttleable liquid rocket engines.

Nomenclature

C = absolute velocity, fps
C_m = axial velocity component, fps
C_u = tangential velocity component, fps
g = gravitational constant, ft/sec²
k = cavitation number, $k \equiv (p_1 - p_v)/(\rho_1 W_1^2/2)$
l = cavity length, ft
N = speed, rpm
p = static pressure, psf
P = stagnation pressure, psf
Δp = pressure rise generated by the pump, psf
Q = delivered system flow, gal/min
r = radius, in.
S_s = critical suction specific speed, $S_s \equiv NQ^{1/2}/(NPSH_{cr})^{3/4}$
U = blade speed, fps
W = inlet flow velocity relative to the blade (see Fig. 3), fps
$NPSH$ = Net positive suction head upstream of injection system and pump, $NPSH \equiv (P_t - p_v)/\rho$
α = incidence angle, angle between the inlet relative velocity and the blade, deg
β = blade angle, angle between the blade and the plane of rotation, deg
γ_j = axial injection angle (see Fig. 6), deg
γ' = flow angle between the absolute velocity of the main flow and the axis of rotation (see Fig. 4), deg
λ_1 = local tangential velocity ratio at pump inlet, $\lambda_1 \equiv C_{u_1}/U_t$ dimensionless
Φ_1 = local flow coefficient at the pump inlet, $\phi_1 \equiv C_{m_1}/U_t$ dimensionless
Φ = system flow coefficient (C_m based on delivered system flow and pump annular flow area) dimensionless
ψ = head coefficient of the pump, $\psi \equiv \Delta p/(\rho U_t^2/2)$ dimensionless
ρ = fluid density, lb/ft³ or slugs/ft³
σ = solidity, a ratio of the blade chord to the blade spacing (in plane of rotation) dimensionless
τ = cavitation coefficient, related to pump $NPSH$, $\tau \equiv (P_t - p_v)/(\rho U_t^2/2)$ dimensionless
ξ = radius ratio, $\xi \equiv r/r_t$ dimensionless
ξ_h = hub ratio, $\xi_h \equiv r_h/r_t$ dimensionless
$(\ )'$ = flow conditions with prerotation

Subscripts

c = cavity
cr = critical
d = design
h = hub
j = injection jet
m = mean, main flow
t = total, tip
v = vapor
1 = inlet
2 = exit

Introduction

MANNED lunar space missions will require propulsion systems providing a wide range of thrust levels.[1, 2] Thrust variations needed may be 2:1 (throttling ratio) for controlling vehicle acceleration or velocity, 5:1 for orbital rendezvous maneuvers, 10:1 for lunar landing, and as high as 25:1 for multiple maneuvers requiring midcourse corrections and trajectory control. These requirements could be met by multiple-thrust rocket engines, but a better solution is a single controllable-thrust rocket engine capable of high throttling ratios.

Rocket engine thrust can be controlled by varying the fuel and oxidizer flowrates directly by controlling pressure, area, or density. With conventional fixed-area injectors with upstream propellant-valve throttling (pressure control), ratios up to 3:1 are readily obtained, and ratios greater than 10:1 can be obtained with unique types of injectors. In the area-control method, the available area is restricted either at the injector or at the thrust chamber nozzle, and achievable throttling ratios are above 25:1. The density-control method consists of injecting low-density inert gas into the propellant to maintain inlet injector pressure and pressure drop.[2] With gas injection in combination with injector area control, deep throttling ratios $\geq$ 50:1 could be obtained. Extensive throttling by any of these methods imposes de-

Presented as Preprint 63-269 at the AIAA Summer Meeting, Los Angeles, Calif., June 17–20, 1963; revision received August 14, 1964. This paper presents results of some basic studies performed under the sponsorship of Headquarters, Ballistic System Division, Air Force System Command. The authors gratefully acknowledge the interest and guidance provided by A. J. Acosta of California Institute of Technology and G. F. Wislicenus of Pennsylvania State University, and the assistance provided by Charles N. Jennings Jr. in conducting the study.

* Senior Technical Specialist, Advanced Projects Department, Rocketdyne Division. Member AIAA.

† Supervisor, Advanced Projects Department, Rocketdyne Division.

‡ Research Engineer, Turbomachinery Analysis Section, Rocketdyne Division.

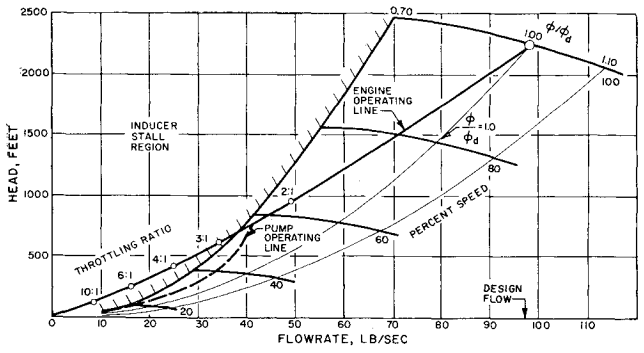

Fig. 1 Performance curves for a typical liquid oxygen pump.

sign and performance problems on both engine components and the vehicle system.

A typical, variable-thrust application might be a liq.O_2/liq.H_2 engine with a 10:1 throttling ratio delivering a large payload on a lunar landing mission. The engine should be able to maintain a constant engine mixture ratio with substantial injector pressure drops relative to chamber pressure to retain high-combustion performance. Additional requirements might include multiple restart capability, rapid cutoff with smooth thrust termination, and minimum pump-inlet suction pressures.

The engine system characteristic determines the equilibrium operating point and operating line (during thrust build-up) for the pump. This is illustrated in Fig. 1 for a liquid-oxygen pump and will be similar for the liquid-hydrogen pump. For a constant-thrust engine, the propellant pumps are designed to operate primarily at the rated (nominal) thrust, and optimum pump-inlet conditions are maintained as the pump accelerates from low speed by following the line for $\Phi/\Phi_d = 1.0$, where Φ is the flow coefficient, defined by the ratio of axial flow velocity entering the pump to pump tip speed ($\Phi \equiv C_{m_1}/U_t$), and Φ_d is the design value for this ratio. For a throttleable engine, the propellant pumps will be forced to operate for extended periods at $\Phi/\Phi_d < 1.0$ along an equilibrium line (heavy curve) that will produce severe off-design conditions for the pump. As the throttling ratio of 2:1 is approached, the pump is operating at $\Phi/\Phi_d \simeq 0.70$, and an area of performance known as the stalled region is approached. With deep throttling (e.g., 10:1), the flow coefficient will fall substantially below its design value, the pump hydrodynamic flow will become highly unstable, efficiency will be poor, and greater inlet-suction pressure to the pump will be necessary to avoid cavitation.

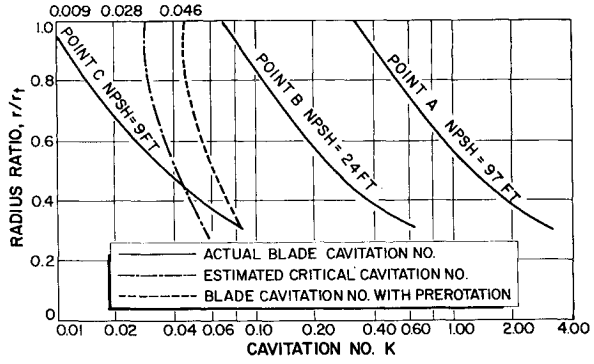

Fig. 2 Blade cavitation number profiles: A, no cavitation; B, partial cavitation; C, full cavitation, and effect of prerotation. (Inducer characteristic: $\Phi_d = 0.114$, $\psi_d = 0.215$, $\xi_h = 0.273$, $\sigma_m = 2.43$, $\beta_m = 15°$.)

The pressure oscillation amplitude of a pump in stall may be nearly twice that at the design flow and, if cavitation is also occurring, it may be magnified again as much as five times. These unsteady phenomena may either excite resonance in the rocket vehicle structure, damage critical vehicle components, or overload the vehicle thrust-control system. To avoid stall and cavitation, the pump operating line must be shifted back into the unstalled region, as shown by the dotted curve in Fig. 1, without affecting the engine operating line or seriously affecting the engine thrust or performance. This paper describes an experimental investigation on a method of fluid injection for a turbopump which will potentially solve these problems.

Effect of Tangential Fluid Injection

The inducer on a pump is an axial-flow element, whose blades are generally designed with nonuniform radial work distribution. It is quite susceptible to adverse pressure gradients,§ and hence to flow reversals at the inlet tip and exit hub. When the pump operates far below Φ_d, the inducer blade stalls at the tip because of the high incidence angle α, which increases as axial velocity is reduced. The high relative velocities and high incidence angles at the blade-tip region combine to lower the local static pressures, thus making the blade also susceptible to cavitation. A potential solution is to control the velocity distribution and increase the fluid pressure of the flow entering the pump by injecting into it a part of the high-pressure fluid from the pump discharge. This effects a momentum transfer to raise the energy level of the flow ahead of the pump. Tangential injection in the direction of blade rotation imparts an angular momentum (prerotation) to the main flow, which reduces both the blade relative velocity and incidence angle. Increasing the effective flow through the pump also reduces the incidence angles. This approach is convenient because injection of high-pressure fluid is simply effected at the pump periphery, where the hydrodynamic problem predominates, and the use of part of the pump discharge flow for this purpose increases the flow entering the pump relative to its output at high throttling ratios.

A two-dimensional cascade analysis using the cavitation number k, which is a parameter that describes blade cavitation in turbomachines,[4] will illustrate the effect of prerotation on inducer inlet flow and cavitation performance. Assuming steady axisymmetric flow and constant axial velocity (with radius) at the inducer inlet, cavitation number profiles on the blade of an experimental inducer were computed for three different inlet pressures p_1 which corresponded to noncavitating (incipient), moderately cavitating (partial), and fully cavitating conditions for the inducer with inlet net positive suction heads $NPSH$ of 97, 24, and 9 ft, respectively (Fig. 2). The curves were computed from

$$k = (p_1 - p_v)/\rho W_1^2/2 = (\tau - \Phi_1^2)(1 + \Phi_1^2)^{1/2} \quad (1)$$

where k is based on upstream static pressure p_1, vapor pressure of the fluid p_v in the flow cavity, and the inlet relative-velocity dynamic pressure $\rho W_1^2/2$; τ is the cavitation coefficient and is directly related to the net positive suction head of the inducer; and Φ_1 is the local flow coefficient radially along the blade. The blade cavitation number is an inverse index to

§ Generally, an inducer has a small number of blades of large chord and small blade angle β and is characterized by low Φ_d and low head coefficient ψ_d. The blades are typically helical, constant pitch, and of high solidity, and their contours will vary with radius according to $r \tan\beta = \text{const}$. Analyses[3] have indicated that this design will reflect strong three-dimensional flows, because the radial boundary-layer flow varies directly with the square of the blade chord (circumferential angle) and varies inversely with the flow coefficient and blade aspect ratio.

cavitation susceptibility. As the inlet static pressure approaches the vapor pressure of the fluid, cavitation will occur or be probable because low k values mean high susceptibility to cavitation. Thus, a low cavitation number is to be avoided.

The k profiles in Fig. 2 are quite steep, and the tip region operates at substantially lower k than the rest of the blade, indicating the high susceptibility of this area to cavitation. To set a limiting cavitation performance for the inducer, the theoretical minimum cavitation number for plane potential flow through a cascade of flat plates[4] was used to estimate the blade critical cavitation number k_{cr}. The minimum cavitation number k_{min} for a blade section with an infinitely long cavity (exceeding the blade chord) was computed from the blade geometry and flow conditions using the relationship¶

$$k_{min} = 2 \sin\alpha \cos(\gamma + \alpha)/(1 + \sin\alpha) \qquad (2)$$

From experimental observations by Acosta,[5] the critical cavitation number for a blade was found to be approximately twice the theoretical minimum value $k_{cr} \simeq 2\ k_{min}$, and the cavity length was finite. Based on this result, the estimated k_{cr} profile for the blade is shown by the dash-dotted curve in Fig. 2. The actual tip cavitation number of $k = 0.009$ for point C is seen to fall far below the estimated critical value of $k_{cr} = 0.028$, and considerable cavitation would be expected in this region (see Fig. 3).

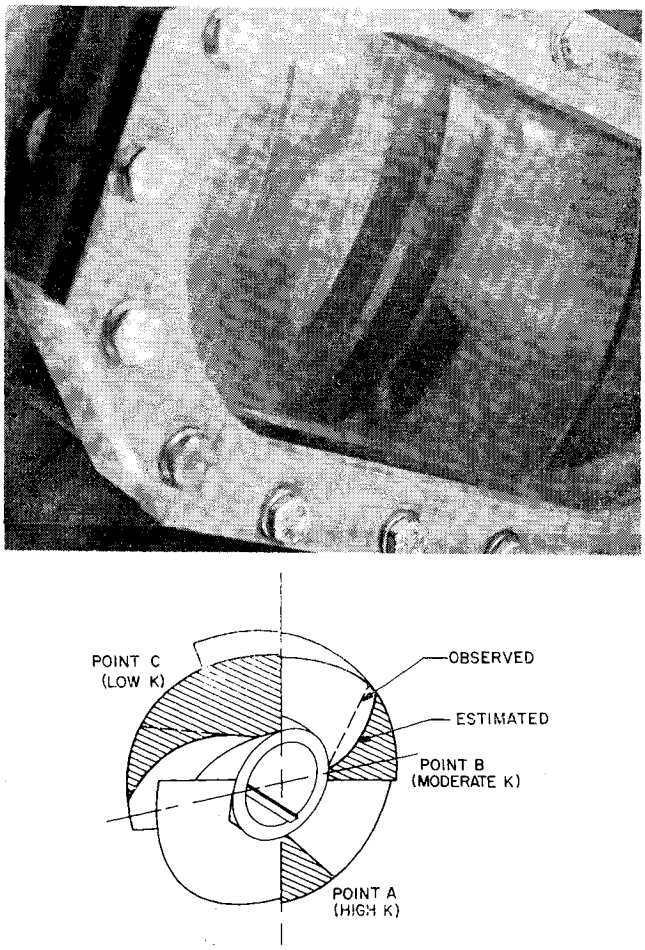

Fig. 3 A comparison of estimated and observed cavity lengths on blade of inducer for operating points A, B, and C. (Photo is typical of partial cavitation on blade for operating point B.)

¶ For small blade angles β and incidence angles α, k_{min} is given approximately by $k_{min} \simeq (\beta - \alpha)$, where $\gamma = (90 - \beta)$.

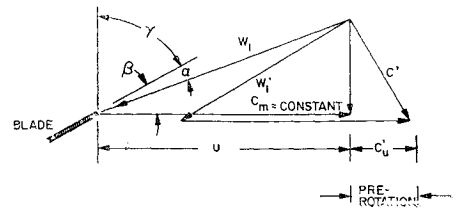

Fig. 4 Velocity diagram with prerotation.

When a tangential component of velocity in the direction of blade rotation C_{u1} is added to the main flow, both the inlet relative velocity W_1 and the incidence angle α of the blade are reduced by this prerotation (Fig. 4). As a result, there is a tendency to raise the operating k and to lower k_{cr}, both of which will increase the blade-cavitation margin. Using some experimental results from a flow study of tangential velocity distributions obtained with fluid injection, a cavitation number profile with prerotation was computed for the inducer for point C with the following relationship:

$$k = (\tau - \Phi_1^2)/[\Phi_1^2 + (1 - \lambda_1)^2] \qquad (3)$$

where λ_1 is the local tangential velocity ratio $\lambda_1 \equiv C_{u1}/U_t$. The resulting k profile (dashed curve in Fig. 2) lies above the critical curve over a large part of the inducer blade and especially at the tip, where k increased from 0.009 to 0.046. As a corollary, the *NPSH* value required to prevent cavitation near the tip is reduced.

Since the inducer encounters critical cavitation long before the length of the cavity on the blade becomes infinite, it would be useful to estimate the size of the cavity to obtain an appreciation for the phenomenon. For this purpose, the theoretical results on partial cavitation in a cascade of flat plates found in Ref. 3 and 4 were used. For free streamline flow on an infinite cascade where the cavity (or free streamline) is attached to the leading edge of the blade, the theo-

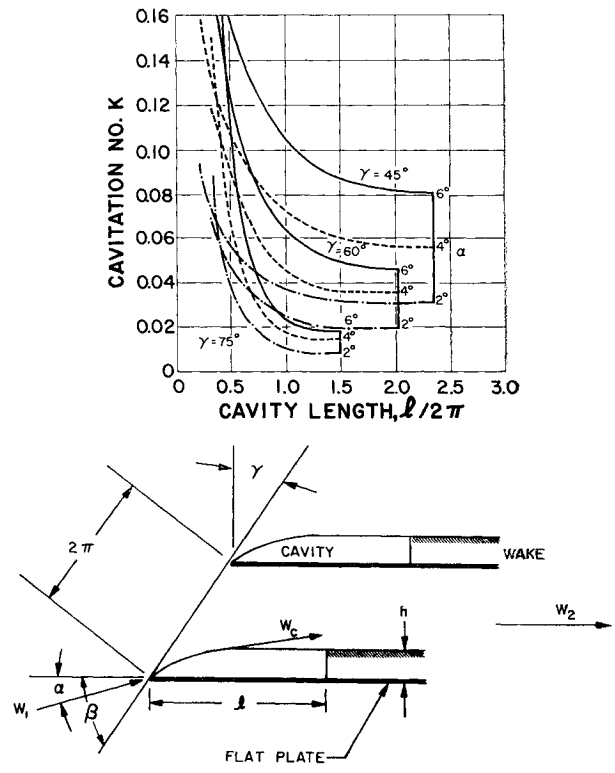

Fig. 5 Theoretical cavity lengths for a flat plate cascade.

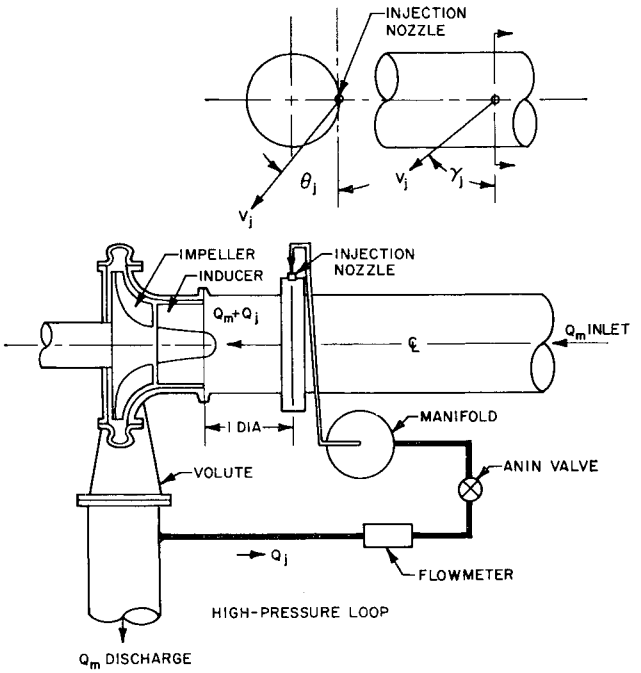

Fig. 6 Schematic of fluid injection loop in pump-test facility.

retical cavity length l (see Fig. 5) is given by the following equation[3] and calculated from cascade geometry and flow:

$$l = \left[\cos\gamma + \left(\frac{W_1}{W_c}\right)^2 \cos(\gamma + 2\alpha)\right] \times \ln\left(\frac{W_c^2 - 2W_1\cos\alpha + W_1^2}{W_c^2 + 2W_1\cos\alpha + W_1^2}\right) - 2\left(\frac{W_1}{W_2} + \frac{W_1W_2}{W_c^2}\right)\cos(\gamma + \alpha)\ln\left(\frac{W_c - W_2}{W_c + W_2}\right) + 2\left[\sin\gamma + \left(\frac{W_1}{W_c}\right)^2 \sin(\gamma + 2\alpha)\right]\tan^{-1}\left(\frac{2W_1W_c\sin\alpha}{W_c^2 - W_1^2}\right) \quad (4)$$

In the forementioned equation, the velocity along the cavity (constant pressure) surface W_c is related to the inlet velocity W_1 by

$$W_c = W_1(1 + k)^{1/2} \quad (5)$$

The estimated cavity length on the inducer blade for the operating points A, B, and C is schematically illustrated and compared with experimental observations in Fig. 3.

Experimental Equipment and Test Facilities

The injection equipment (Fig. 6 and Table 1) was designed to allow the test parameters, injection angle, and location to be varied. The basic parts are an injection ring, nozzle plugs, and nozzles. Three sets of nozzle plugs were used to provide tangential injection angles of 0° (tangential), 15°, and 20° in the plane of rotation (normal to flow). These plugs can be rotated 90° from the plane or rotation into the meridional plane and directed downstream with the main flow. Two test facilities were used: a water tunnel for preliminary work with inducers and a pump-test facility for testing the inducers with injection in a complete pump.

Table 1 Test parameters used in flow study

Geometry	Cases		
Number of nozzles	4	6	12[a]
Nozzle diam., in.	$\frac{1}{8}$	$\frac{3}{16}$[a]	$\frac{1}{4}$
Injection angles, deg			
Tangential, θ_j	0	15[a]	30
Axial, γ_j	0	15[a]	45
Nozzle test conditions	**Cases**		
Pressure drop, psig	20	55	90
Pressure ratio, P_j/p_1	4	9	14
Flow (Q_j/Q_m), %	5	10	15
Injection station, diam	$\frac{1}{2}$	1	$1\frac{1}{2}$
Velocity ratio, V_j/C_m	3.5	6	7.6

[a] The configuration used in the flow study.

The water-tunnel facility is a closed-loop, recirculating tunnel with a horizontal test section, and has a maximum flow rate of approximately 3000 gal/min and a normal operating inducer shaft speed of approximately 6000 rpm. Gaseous nitrogen is used to pressurize the run tank above the test section to a maximum of 135 psig, and a vacuum pump is used to reduce the pressure to a minimum of 24-in. Hg vacuum. The high-pressure, secondary-flow loop for the injection system begins from a tapoff in the tunnel downstream of the test section, bypassing a portion of the flow into a high-pressure, two-stage centrifugal pump. The high-pressure flow is fed into a manifold, which then feeds the individual nozzles in the injection ring.

The test section is made in four parts from clear Lucite stock (6.4-in. i.d. by 1.0-in. wall) to permit visual observations and to allow the injection ring to be placed at the very inlet of the inducer or at any $\frac{1}{2}$-diam increment upstream to a maximum of 2 diam. The test section is instrumented with static-pressure taps and survey probes (Feichheimer directional probes) for flow measurements. A pulse camera (motion picture) provides flow visualization under either frozen or slow-rolling conditions by sending synchronized pulses (generated by an electromagnetic pickup sensing shaft rotation) to both a 25 μsec strobe light and the camera shutter.

The pump-test facility (Fig. 6) is a closed-loop water circuit with a horizontal test section. Flow rates up to 3000 gal/min and shaft speeds up to 17,000 rpm are obtainable. Compressed nitrogen and a vacuum pump are used to regulate pressure. The injection ring is shown located at approximately 1 diam ahead of the pump, and the high-pressure fluid is tapped from the pump-volute discharge.

Discussion of Experimental Results

Two inducers and one complete pump were tested with fluid injection. Below-design performance, during cavitation and noncavitating conditions, and upstream velocity distributions were studied. Obtaining upstream prerotation of the main flow by jet-momentum action is a highly complex fluid mechanics problem, and it would be difficult to predict both the velocity and pressure distributions of two impinging flows[6] and their resulting momentum transfer properties.[7, 8] For the purpose of the present investigation, the radial distributions of C_{m_1}, C_{u_1}, γ, p_1, and P_{t_1} upstream of the pump, together with the effective jet penetration and the influence of mixing loss with axial distance, were directly determined experimentally by varying systematically the test parameters (Table 1).

Flow Distribution Obtained with Fluid Injection

The velocity, flow angle, and pressure distributions obtained $\frac{1}{2}$ diam downstream of the injection point with $\theta_j = \gamma_j = 15°$ are presented in Fig. 7. Typical distributions for injection-pressure ratios of $P_j/p_1 = 2$, 3, and 8 are illustrated. Maximum prerotation was usually obtained at the periphery of the test section. This prerotation diminished rapidly to zero at a radius ratio of 0.40 for high injection-pressure ratios (Fig. 7a). There was a tendency for the inner half of the flow (at centerline) to accelerate and the outer half to decelerate (shown by the C_m distribution in Fig. 7b) because of the blockage effect produced by the injection flow. The

effect was most pronounced at the high injection-pressure ratios. The flow angle and pressure distributions are shown in Figs. 7c and 7d.

The penetration of the jet into the main flow was found to depend mainly on the tangential injection angle θ_j. A depth of only $\frac{1}{2}$ in. was reached with $\theta_j = 0°$ ($\gamma_j = 30°$), whereas penetration to the centerline at (3.2 in.) was obtained with $\theta_j = 30°$ ($\gamma_j = 15°$) within a short distance of the injection point. The decay in prerotation with distance because of mixing losses is shown in terms of flow angles at $\xi = 0.925$ in Fig. 7e.

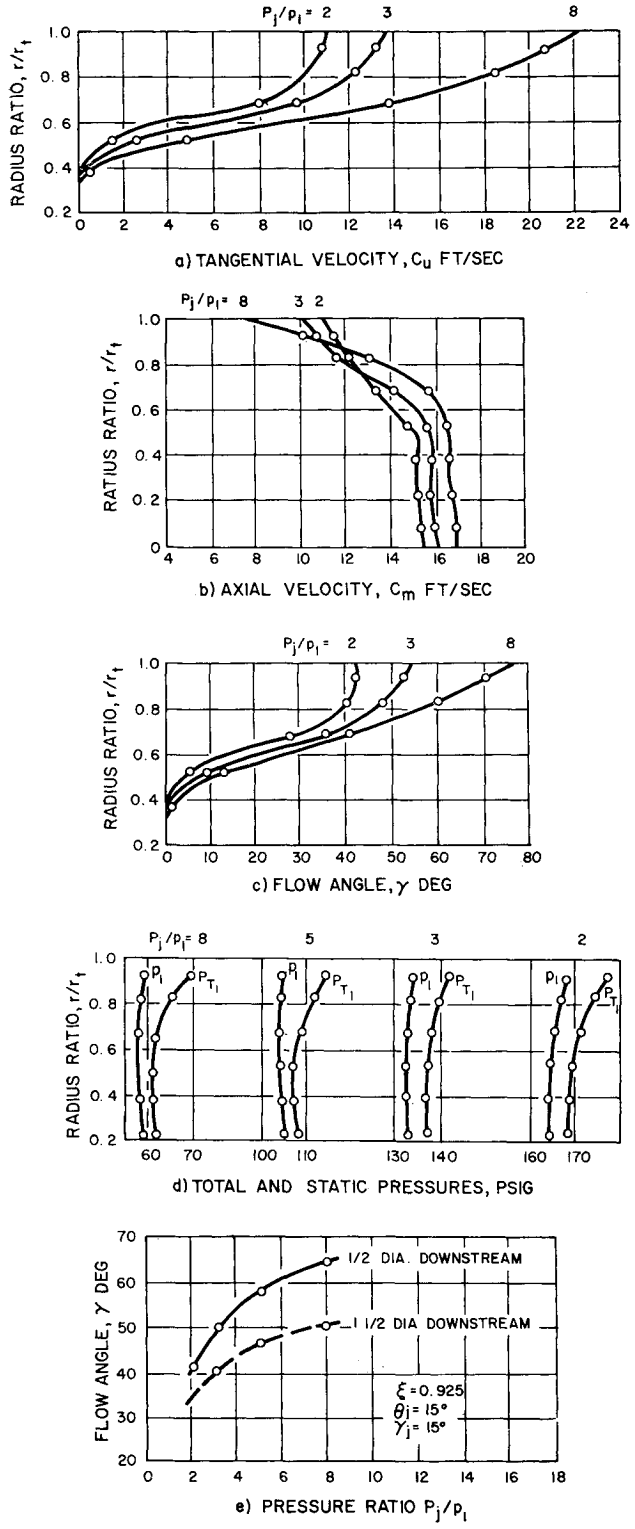

Fig. 7 Flow distribution $\frac{1}{2}$ diam downstream of injection ring, $\theta_j = \gamma_j = 15°$.

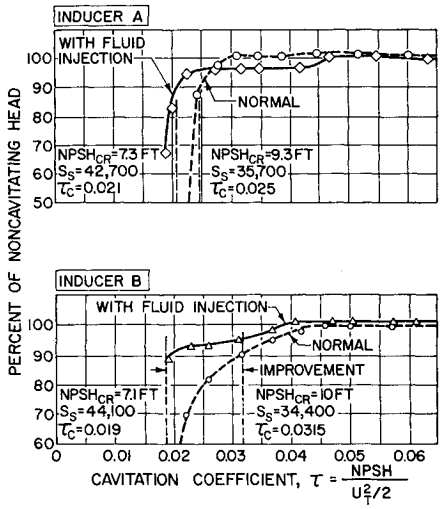

Fig. 8 Inducer suction performance from water tunnel tests with $\theta_j = 0°$, $\gamma_j = 45°$, $\Delta p = 115$ psi. Note gain in τ at 90% system head (the critical point) due to injection.

Cavitation Results for Two Inducers

The design parameters for the two inducers tested with fluid injection in the water tunnel are summarized in Table 2. The injection point was placed at $\frac{1}{2}$ diam upstream of the inducer. The cavitation tests were run at the design flow coefficient at a constant speed and flowrate while the system pressure was lowered. The noncavitating tests were run at constant tunnel pressure and speed.

The increase in inducer suction performance obtained with fluid injection is shown by the test curves in Fig. 8, and the suction performance is based on the lower delivered system flow and the *NPSH* upstream of the injection point. The curves indicate the amount of head lost as the inlet suction pressure (or τ) is reduced. The 90% point is called the critical point, because a 10% system loss corresponds to a 2% loss in head in a complete pump, which is a typical maximum allowable specification for an engine at rated thrust. This point therefore defines the $NPSH_{cr}$. With a nozzle injection angle of $\theta_j = 0°$ and $\gamma_j = 45°$ and an injection flow rate of approximately 9%, the suction performance of inducer *A* increased from a critical suction specific speed

$$S_s = NQ^{1/2}/(NPSH_{cr})^{3/4} \qquad (6)$$

of $S_s = 35{,}700$ without fluid injection to $S_s = 42{,}700$, an increase of 20%. For inducer *B*, S_s increased from 34,400 to 44,100, an increase of 28%. When fluid injection is used, the inducer design flow coefficient ($\Phi_d = 0.08$) represents the lower discharge flow delivered to the engine system by the pump rather than that entering the pump. The actual inducer inlet flow coefficient, therefore, will be higher by the amount of the injection flowrate.

Using the inducer flow analysis described in the previous section, the suction performance of inducer *A* with prerotation may be estimated by computing the blade tip cavitation number. For the normal $NPSH_{cr}$ of 10 ft and the inlet

Table 2 Inducer design data

Inducer	*A*	*B*
Tip diam, in.	6.40	6.40
Hub diam, in.	1.28	1.27
Flow coefficient, Φ_d	0.080	0.084
Head coefficient, ψ_d	0.140	0.123
Solidity, σ_m	2.470	2.140
Blade angle β_m, deg	8.35	7.79

velocity distributions obtained from the flow studies (similar to Fig. 7 for $\theta_j = 0°$ and $\gamma_j = 45°$), prerotation increased the theoretical tip cavitation number by 20% from a critical value of 0.025 to a noncritical value of 0.031. Conversely, for $k_{cr} = 0.025$, prerotation lowered the theoretical $NPSH_{cr}$ to 8.5 ft, and the resulting S_s based on the blade tip increased from 35,000 to 41,000, a gain of 17%, which may be compared to the 20% gain obtained experimentally in Fig. 8. Thus, the simple analysis gives fair agreement with test data. A more exact analysis of the performance over the total blade would be required to give better predictions.

Estimate of Cavitation Performance with Cryogenic Liquids

The cavitation phenomenon is a very complex mechanism, and pump cavitation performance with one liquid will be different from such performance with another liquid, especially between water and cryogenic liquids. Generally, pump cavitation performance with liquid oxygen, liquid nitrogen, and liquid hydrogen is higher than with water. This increase in performance is attributed to a decrease in the liquid temperature during the cavitation (or boiling) process, as heat is taken from the liquid to form the vapor cavities, and the resulting decrease in the vapor pressure is equivalent to an increase in available suction head or $NPSH$ to the pump. Many theoretical models have been proposed for correlating cavitation in terms of the following fluid properties: liquid temperature and pressure, specific heat, specific vapor volume, specific liquid volume, latent heat of vaporization, vapor-to-liquid volume ratio, vapor-to-mixture volume ratio, acoustic velocity of two-phase mixture, thermal conductivity, surface tension, compressibility, etc. Some of the models are the thermostatic model, which uses the parameters of vapor-to-liquid volume ratio (the cavitation tendency number[9] or the cavitation tendency ratio,[10] which may include surface tension effects[11]) and vapor-to-mixture volume ratio[12]; the bubble growth model and its distribution of cavitation nuclei[5, 13]; and the acoustic-shock model.[14]

Since it is important to consider the extent of cavitation in a turbomachine, and the cavitation phenomenon is so complex, it is not surprising that no single model has predicted pump cavitation in different liquids accurately. More theoretical studies would be required to relate the basic effects of thermostatics, bubble growth dynamics, surface tension, heat transfer, nuclei concentration, etc., with the three-dimensional flow in the turbomachine. However, it has been found from studying experimental data that pump cavitation performance with liquid oxygen is approximately 1.2 times greater than water,[14] and with liquid hydrogen it is greater by a larger factor. Thus, inducer A with fluid injection would have a S_s of 51,200 with liquid oxygen and would be even higher with liquid hydrogen.

One additional factor to consider when the pump discharge flow is used for fluid injection is the temperature rise acquired by the liquid across the pump. As the rate of change of vapor pressure with temperature is significant with cryogenic liquids, the temperature of the flow entering the pump after mixing will directly affect the cavitation performance. Although a detailed study has not been made on the net effect of this factor for various conditions, available test data approximating this condition indicate that some loss in performance should be expected.

Noncavitating Performance

Typical noncavitating performance (head-capacity curves) for inducers A and B with fluid injection is shown in Fig. 9 in the dimensionless terms of head and flow coefficients (these curves are independent of speed). Recalling that in Fig. 1 the pump operating line must fall to the right of the engine operating line at high throttling ratios to prevent stalling, one can see the stall margin obtained with fluid injection in Fig. 9. The first solid curve represents points of lower flowrates delivered to the engine system, because a portion of the high-pressure flow has been bypassed for fluid injection. The second solid curve represents inducer operating points close to its design condition (dotted curve) at the higher flow coefficients made possible by using the bypass flow for fluid

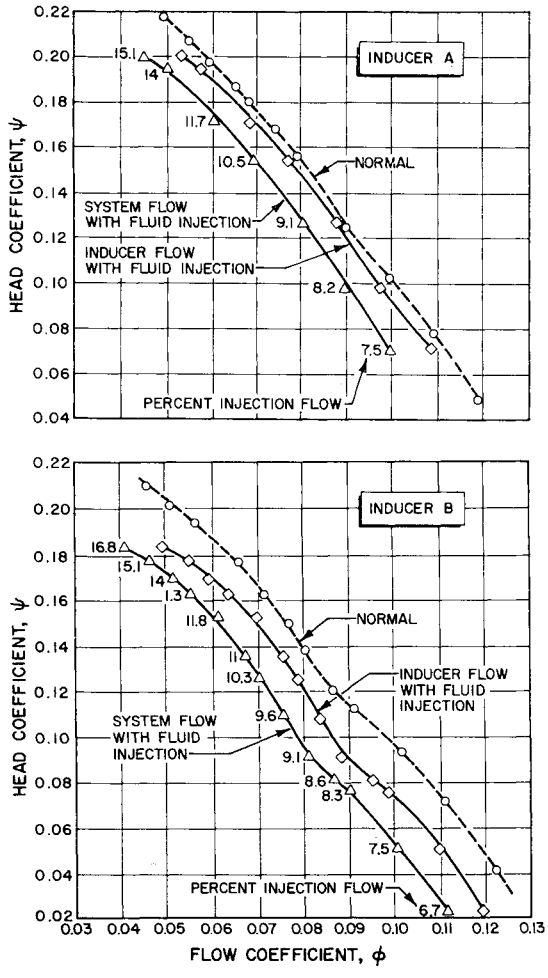

Fig. 9 Inducer head-capacity curves from water-tunnel tests with $\theta_j = 0°$, $\gamma_j = 45°$, $N = 5500$ rpm.

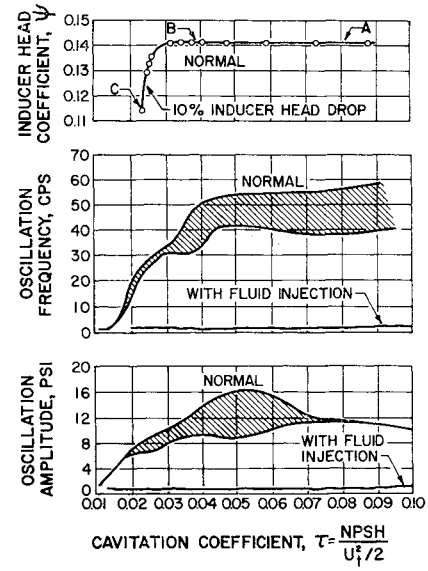

Fig. 10 Flow oscillations for inducer A with and without fluid injection.

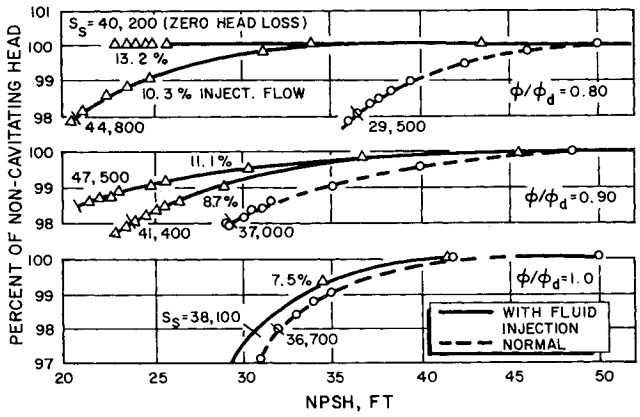

Fig. 11 Pump suction performance at various injection flowrates with $\theta_j = 0°$, $\gamma_j = 60°$.

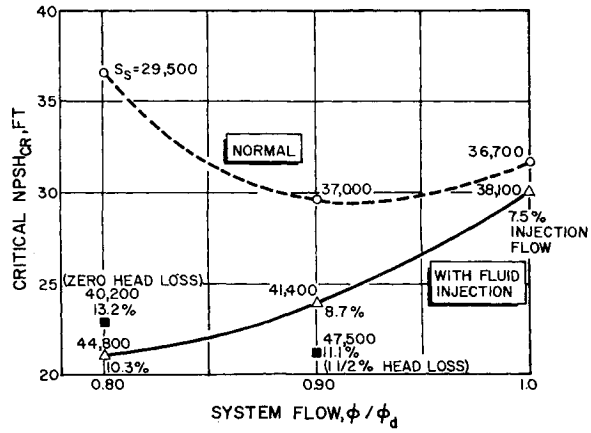

Fig. 12 Reduction in pump net positive suction head requirement at 2% head loss with fluid injection for system flow below the design value ($\Phi/\Phi_d < 1.0$).

injection. Injection angle, injection pressure ratio, and nozzle size may be varied to obtain different head-capacity characteristic curves.

Flow Stability

Typical flow oscillations for inducer *A* are shown in Fig. 10. Both the oscillation amplitude and frequency are significantly reduced when inlet fluid injection is used, since cavitation is suppressed until lower suction pressures are reached. (The reduction in cavitation intensity also was evident from the pronounced lessening of cavitation noise and structural vibration to the test stand.) Similarly, during noncavitating conditions unstable flow also was avoided when fluid injection prevented inducer stall and flow reversals at low flow coefficients.

Pump-Test Results

To investigate the effect of fluid injection on the experimental pump (Table 3) in the pump facility, the high-pressure fluid (water) was taken directly from a bypass at the discharge of the pump volute (see Fig. 6). The injection ring was placed 1 diam upstream of the pump (which has an inducer element). The test procedure for obtaining cavitation and noncavitating performances was similar to the inducer tests.

The test results for $\Phi/\Phi_d = 0.8$, 0.9, and 1.0 are presented in Figs. 11 and 12. The pump speed was 10,000 rpm, and nozzle injection angles were $\theta_j = 0°$ and $\gamma_j = 60°$. The critical net positive suction head in this case is defined at the point of 2% loss in total pump head as a result of cavitation. One can see that, at the off-design point of $\Phi/\Phi_d = 0.80$, the suction performance (Fig. 11) is poorest or the *NPSH* required is highest (Fig. 12). It was for this point that fluid injection had the greatest effect. With an injection flowrate of 10.3%, S_s was increased from 29,500 to 44,800, an increase of 52%, and $NPSH_{cr}$ was decreased from 36 to 21 ft. High injection flowrates generally were found to give high suction performances. At this same off-design point with an injection flowrate of 13.2%, the facility vacuum system was not able to lower the pump inlet pressure enough to cause cavitation. As a result, $S_s = 40{,}200$ was obtained with no loss in pump head. Figure 12 clearly illustrates the normal off-design *NPSH* requirements of the pump and the reductions obtained with fluid injection.

In the noncavitating tests, the pump was able to operate close to its design point with fluid injection while delivering a lower flowrate to the system. The pump discharge pressure oscillation amplitudes (measured with photocon pressure transducers), normally ranging from 30 to 40% of the discharge pressure, were found to be reduced in half with nozzle injection angles of $\theta_j = 0°$ and $\gamma_j = 60°$ or 75°. No measurable amplitudes were recorded by the pressure transducers for $\gamma_j = 45°$.

Table 3 Experimental pump parameters for water test in pump facility with twelve $\frac{3}{16}$-in. nozzles 1 diam upstream

Experimental pump	Inducer	Pump
Flow coefficient, ϕ_d	0.106	...
Head coefficient, ψ_d	0.087	0.455
Solidity, σ_m	2.53	...
Blade angle β_m, deg	15.75	...
Diam, in.	6.06	7.50
Injection system		
θ_j, deg = 0 γ_j, deg = 45, 60, 75		
Test conditions		
N, rpm = 10,000 Q_m, gal/min = 1950, 2190, 2440 Q_j gal/min = 140 to 258		

Concluding Remarks

This experimental investigation demonstrated the feasibility of using tangential high-energy fluid injection, operating from a bypass system, to solve the off-design performance problems in a pump-fed propellant rocket engine requiring high throttling ratios. Although no attempt was made to simulate specific engine requirements (and water was the only test fluid), sufficient test data were obtained with a simple injection system and pump components to establish the merits of the concept for throttleable engines using either storable or cryogenic liquid propellants. The results from the inducer and pump tests have demonstrated that fluid injection can 1) maintain near-design flow conditions to the turbopump while substantial reduction in engine flowrate occurs during throttling; 2) lower the turbopump *NPSH* (or system pressurization) requirement at off-design flowrates by suppressing cavitation; and 3) reduce the potentially destructive effects of flow instabilities or oscillations in the turbopump. Furthermore, the ability to control pump inlet energy and flow distribution by fluid injection (prerotation) also suggests the possibility for optimizing blade design with respect to off-design performance.

References

[1] Welton, D. E., Bensky, S. M., and Hiland, J. R., "Toward the variable-thrust liquid-rocket engine," Astronaut. Aerospace Eng. 1, 77–81 (December 1963).

[2] Coultas, G. A., "Controllable thrust rocket engines: applications and techniques," Society of Mechanical Engineers Meeting, Los Angeles, Calif. (March 1963).

[3] Ghahremani, F. G., MacGregor, C. A., and Wong, G. S., "A study of various methods for suppressing cavitation in rotating fluid machines," Wright Air Development Center TR 59-411, p. 39 (June 1959).

[4] Acosta, A. J. and Hollander, A., "Remarks on cavitation in turbomachines," Engineering Div., California Institute of Technology, Pasadena, Calif., Rept. 79.3 (October 1959).

[5] Acosta, A. J., "An experimental study of cavitating inducers," Second Symposium on Naval Hydrodynamics, Washington, D. C. (August 1958).

[6] Torda, T. P. and Stillwell, H. S., "Analytical and experimental investigations of incompressible and compressible mixing of streams and jets," Wright Air Development Center TR 55-347 (March 1956).

[7] Gosline, J. E. and O'Brien, M. P., "The water jet pump," *University of California Publications in Engineering* (University of California Press, Berkeley, Calif., 1942), Vol. 3, pp. 1–28.

[8] Cunningham, R. G., "Jet pump theory and performance with fluids of high viscosity," J. Basic Eng. **79**, 1807–1820 (1957).

[9] Stepanoff, A. J. and Stahl, H. A., "Thermodynamic aspects of cavitation in centrifugal pumps," Trans. Am. Soc. Mech. Engrs. **A78**, 1691–1693 (1956).

[10] Boretz, J. E., "Use of cavitation tendency ratio for predicting suction specific speed," AIAA J. **1**, 453–454 (1963).

[11] Jacobs, R., Martin, K., Van Wylen, G. J., and Birminghan, B. W., "Pumping cryogenic liquids," U. S. Dept. of Commerce, National Bureau of Standards, Rept. 3569, Boulder Labs., Boulder, Colo. (February 1956).

[12] Salemann, V., "Cavitation and NPSH requirement of various liquids," Trans. Am. Soc. Mech. Engrs. **D81**, 167–173 (June 1959).

[13] Sarosdy, L. R. and Acosta, A. J., "Note on observations of cavitation in different fluids," American Society of Mechanical Engineers Paper 60-WA-83 (December 1960).

[14] Jakobsen, J. K., "On the mechanism of head breakdown in cavitating inducers," Trans. Am. Soc. Mech. Engrs. **D86**, 291–305 (1964).

JAN.-FEB. 1965 J. SPACECRAFT VOL. 2, NO. 1

Cost and Weight Optimization for Multistage Rockets

J. S. GRAY* AND R. V. ALEXANDER†
Aerojet-General Corporation, Sacramento, Calif.

A mathematical procedure is derived whereby optimum staging for minimum cost may be computed, with minimum weight staging obtained as a special case. Fixed costs and costs that vary with motor weight are considered in the solution. The results produce minimum-cost staging either for fixed payload or for fixed launch weight. Problems of minimum-weight staging for a fixed payload or maximum-payload staging for a fixed launch weight may also be treated by this analysis. All solutions are subject to the constraint of a fixed, predetermined, ideal velocity. Structural efficiency (propellant fraction, Λ) and motor costs are considered variables that depend on the stage number and size. Minimum-cost staging is compared with minimum-weight staging, ideal staging, and various intermediate possibilities. The optimization procedure is demonstrated with hypothetical vehicles; it applies equally to solid, liquid, and nuclear rockets.

Nomenclature

C = cost per pound of motor, a function of motor mass, \$/lb
$C_{\min}$ = asymptotic cost, an empirical constant, \$/lb
C_T = total vehicle cost, \$
CT = total system cost, for system with divisible payload, \$
FC = fixed cost per launch, \$
g_c = gravity conversion factor, ft-lbm/lbf-sec^2
I_s = specific impulse, lbf-sec/lbm
M = motor mass, including interstage structure, lbm
M_b = mass of vehicle at propellant burnout, lbm
M_0 = initial mass of vehicle stage, lbm
M_L = mass of vehicle payload, lbm
M_p = propellant mass, lbm
N = number of stages for multistage rocket
n = number of launches for a divisible payload
PL = total system payload, for system with a divisible payload, lbm
v_{ib} = total ideal velocity increment = $\sum_i^N \Delta V_i$, fps
ΔV_i = ideal velocity increment of the ith stage, fps
$\eta, \eta^*, \hat{\eta}$ = Lagrange multipliers
k_j = empirical constants, $j = 1, 2, 3, 4$
Λ = propellant fraction, a function of motor mass $\equiv M_p/M$
$\Lambda_{\max}$ = asymptotic propellant fraction, an empirical constant

Received May 12, 1964; revision received August 21, 1964. The authors wish to acknowledge the contributions of R. Q. Fong to the subject of this paper and J. M. Chapp for preparation and editing.

* Development Engineer, Exterior Ballistics and Design Optimization Section, Applied Mechanics.

† Senior Engineer, Exterior Ballistics and Design Optimization, Applied Mechanics. Member AIAA.

Introduction

RECENT emphases in very ambitious space missions have brought about a new interest in the cost of staging the rocket propulsion system. The objective of this paper is to present an analytic method of staging multistage rockets to arrive at a minimum-cost system and, as a special case, a minimum-weight system.

Several papers[1–5] have been written in which vehicle staging for minimum weight or minimum cost has been the objective. Fixed costs were considered in two of these,[2, 3] and propellant fraction expressed by a nonlinear relationship with motor weight was considered in one.[1] However, motor cost beyond linear relationships was not considered in any of the referenced material. The following examples show the need for just such an optimization procedure.